HHS Public Access

Author manuscript

Biomaterials. Author manuscript; available in PMC 2019 August 01.

Published in final edited form as:

Biomaterials. 2018 November ; 183: 295–305. doi:10.1016/j.biomaterials.2018.07.059.

Guided tissue organization and disease modeling in a kidney tubule array

Balajikarthick Subramanian[a,b,**], **Oguzhan Kaya**[a], **Martin R. Pollak**[b], **Gang Yao**[a], **Jing Zhou**[a,c,*]

[a]Harvard Center for Polycystic Kidney Disease Research and Renal Division, Department of Medicine, Brigham and Women's Hospital, Harvard Medical School, Boston, MA, USA

[b]Division of Nephrology, Beth Israel Deaconess Medical Center, Boston, MA, USA

[c]Harvard Stem Cell Institute, Cambridge, MA, USA

Abstract

Three-dimensional (3D) *in vitro* kidney tubule models have either largely relied on the self-morphogenetic properties of the mammalian cells or used an engineered microfluidic platform with a monolayer of cells cultured on an extracellular matrix (ECM) protein coated porous membrane. These systems are used to understand critical processes during kidney development and transport properties of renal tubules. However, high variability and lack of kidney tubule-relevant geometries among engineered structures limit their utility in disease research and pre-clinical drug testing. Here, we report a novel bioengineered guided kidney tubule (gKT) array system that incorporates *in vivo*-like physicochemical cues in 3D culture to reproducibly generate homogeneous kidney tubules. The system utilizes a unique 3D micro-molded ECM platform in human physiology-scale dimensions (50-μm diameter) and relevant shapes to guide cells towards formation of mature tubule structures. The guided kidney tubules in our array system display enhanced tubule homogeneity with *in vivo*-like structural and functional features as evaluated by marker protein localization and epithelial transport analysis. Furthermore, the response of gKT structures to forskolin treatment exhibits characteristic tissue transformations from tubules to expanding cysts. Moreover, acute cisplatin injury causes induction of Kidney Injury Molecule-1 (KIM-1) expression as well as tubular necrosis and apoptosis. Thus the gKT array system offers enhanced structural uniformity with accurate *in vivo*-like tissue architecture, and will have broad applications in kidney tubule disease pathophysiology (including ciliopathies and drug-induced acute kidney injury), and will enhance pre-clinical drug screening studies.

[*]Corresponding author. Harvard Institutes of Medicine, 4 Blackfan Circle, Room 522, Boston, MA 02115, USA. jzhou@bwh.harvard.edu, jingzhoubwh@gmail.com (J. Zhou). [**]Corresponding author. 99 Brookline Avenue, RN320, Boston, MA 02215, USA. bsubram1@bidmc.harvard.edu (B. Subramanian).

Contributions

Balajikarthick Subramanian: Conceived the idea, managed the study, performed the experiments, analyzed the data and wrote the manuscript. Oguzhan Kaya and Gang Yao: Performed the experiments and reviewed the manuscript. Martin Pollak: Analyzed the data and edited the manuscript. Jing Zhou: Conceived the idea, directed and managed the study, analyzed the data and edited the manuscript.

Disclosure of conflicts of interest

None.

Appendix A. Supplementary data

Supplementary data related to this article can be found at https://doi.org/10.1016/j.biomaterials.2018.07.059.

Keywords

Bioengineering; Kidney tubule array; 3D culture; Cystic kidney disease; Acute kidney injury; Cilia

1. Introduction

Animal models - the current gold standard for disease modeling - are commonly believed to have physiological relevance to various human kidney diseases [1,2]. However, dissecting the cellular events leading to disease is often complex and unclear, hindering drug discovery [1,2]. Three-dimensional (3D) cellular systems can recreate *in vivo*-like complexity and are amenable to dissection of cellular events associated with disease processes, thus complementing various animal models [3–5]. In addition, 3D systems can be adapted for use in high-throughput screening, as the case with two-dimensional (2D) cell culture systems [3].

Kidney tubules require a complex set of physical and chemical cues that facilitate the maintenance of accurate tissue geometry and function [6]. Previous studies have shown that structural and functional qualities of tubules including transport functions begin early in kidney development and that serially-reaggregated engineered embryonic kidneys *in vitro* exhibit similar structure and transport functions as well [7]. Over the last few years, multiple systems have been developed to mimic this complex regulation *in vitro* and to construct 3D kidney tubule structures and functions to aid in disease understanding and drug development [8–11]. Many of these systems have relied on self-morphogenetic properties of the mammalian cells, as exemplified by spheroids and organoids, or have used cell monolayers cultured on extracellular matrix (ECM) protein-coated porous membrane in a microfluidic device to simulate kidney tubule –like transport [9–11]. While the self-morphogenetic systems are useful to understand kidney tubule morphogenesis, they lack homogeneous structures and control over tissue geometry, increasing the difficulty of interpretation of outcomes and high-throughput screening assay development. In contrast, conventional microfluidic systems are useful for understanding tubular transport, but the lack of 3D organization does not allow for tubule structure-related investigations.

There is a need to develop a tubule model system for kidney disease research and drug testing that bridges the gap between animal models and 2D cell systems, including both the chemical cues from ECM (to mediate important ECM signaling pathways) and the physical cues of tissue geometry (to develop appropriate, homogenous morphology). While matrix components such as collagen I or matrigel can provide cells with the necessary milieu, imposition within the matrix of geometrically defined 3D tissue-like patterns can provide the necessary physical cues to establish homogenous tissue geometry.

Therefore, in the present study, we employed soft- and photolithography based procedures to prepare a unique 3D micropatterned ECM platform with features in the size and shape ranges of human physiology for development of human kidney tissue models. We report for the first time, the recapitulation of functional human kidney tubules in an array platform. Furthermore, the developed tissue array offers *in vivo*-like structural homogeneity and complexity in its ECM components and tissue geometry. We suggest that this 3D tissue array

will be valuable in the study of human kidney disease pathophysiology and drug testing applications.

2. Materials and methods

2.1. Cell culture

Mouse Inner Medullary Collecting Duct cells (mIMCD3 cells) (CRL-2123, ATCC, VA) were maintained in Dulbecco's Modified Eagle Medium: Nutrient Mixture F-12 (DMEM/F12) (Invitrogen, CA) supplemented with 10% fetal bovine serum (Invitrogen, Carlsbad, CA) and 1% pen-strep (Invitrogen, CA). Human proximal tubule cells (HK-2) (CRL-2190, ATCC, VA) were maintained in Keratinocyte Serum Free Medium (K-SFM) (17005–042, Invitrogen, CA) supplemented with0.05 mg/mL bovine pituitary extract, 5 ng/mL epidermal growth factor, 2.5% fetal bovine serum (Invitrogen, CA) and 1% pen-strep (Invitrogen, CA). Human embryonic kidney epithelial cells (293 cells) were maintained in Dulbecco's Modified Eagle Medium supplemented with 10% fetal bovine serum (Invitrogen, Carlsbad, CA) and 1% pen-strep (Invitrogen, CA).

2.2. Tissue geometry microfabrication and guided kidney tubule (gKT) array set up

Tissue geometry micropatterns were designed in AutoCAD and transferred as topographic patterns in polydimethylsiloxane (PDMS) (Dow Corning, MI) using a combination of photolithography and soft lithography techniques as described previously [12]. The dimensions of the topographic patterns used in this study were 50 × 200 × 50 μm (Width X Length X Height).

For initiating gKT system, a well of 1 × 1 × 0.5 cm (Length X Breadth X Depth) was cast on top of a glass slide (or coverslips) using blank cured PDMS. The well was filled with ECM, and the stamp with preprogrammed kidney tubule features was placed on top of it. Following ECM gelation for 30 min at 37 °C, the stamp was removed gently, and the features are now replicated to the ECM hydrogel. Quantitative profiling of human kidney ECM has shown that collagen IV, laminin and collagen I are the major components of kidney ECM [13]. As matrigel comprises mainly collagen IV and laminin, we have exclusively used collagen I and matrigel based ECM components. Thus, the following ECM combinations were used to replica mold the kidney tubule features from the PDMS stamp: Collagen type I (High concentration Rat Tail, Corning, MA, Cat No: 354249) 3 mg/mL; Matrigel (growth factor reduced LDEV free, Corning, MA, Cat No: CB356252); Collagen-Matrigel (Collagen I 3 mg/mL final plus matrigel 50% by volume).

To initiate cultures, cells were prepared as single cell suspensions at 3×10^6 cells/mL, added to the replica-molded ECM and pelleted within the features by centrifugation at 500*g* for 3 min. The orientation was ensured that length of the patterns was perpendicular to the rotational axis during centrifugation. Post centrifugation, excess cells were gently washed away with phosphate buffered saline (PBS), and a second top layer (of 50 μm thickness) of the same ECM was allowed to gelate for another 30 min. The system was then incubated with appropriate cell media and allowed to form gKT structures. All analyses on gKT structures were performed on day 4 or day 5.

2.3. Treatments

mIMCD3 based gKT structures were incubated with forskolin (Sigma, MO) (30 μM) starting on day 3 for a period of 48 h. For drug-responsive groups, gKTs were pre-incubated for 8 h with Na-K-Cl co-transporter (NKCC) inhibitor, Bumetanide (50 μM) (Sigma, MO), followed by co-incubation with forskolin. For cisplatin treatments, gKT structures of HK-2 cells were treated with the indicated concentrations (5, 10 or 20 μM) starting on day 4 for a period of 24 h.

2.4. Organic anion and cation transport

gKT structures of HK-2 cells were incubated in basal keratinocyte serum-free medium for 30 min followed by addition of the organic anion, 6-carboxyfluorescein (6-CF) (2 μM) (Sigma, MO) and Propidium Iodide (2 μM) (PI, Invitrogen, CA) for 45 min [5]. Following the uptake incubation, gKT structures were PBS-washed three times and imaged as an unfixed system by confocal microscopy. For inhibitor groups, gKT structures were pre-incubated with 2 mM organic anion transport (OAT) inhibitor, probenecid (Sigma, MO) for 2 h followed by co-incubation with 6-CF and PI. To quantitate uptake, the gKT HK-2 structures were digested with collagenase A (2 mg/mL) (10103586001; Hoffmann-La Roche, NJ) for 30 min, lysed in RIPA (Radio-Immunoprecipitation Assay) buffer and assayed by fluorescence plate reader (Spectra Max M series, Molecular Devices, CA) at 488 nm excitation and 525 nm emission. The fluorescence values were normalized to protein (BCA assay, Bio-Rad, CA).

Similarly, for organic cation transport analysis, gKT structures were incubated in basal keratinocyte serum-free medium for 30 min followed by addition of organic cation, rhodamine-6G (50 μM) (Sigma, MO) for 1 h. For inhibitor groups, gKT structures were pre-incubated with 500 μM organic cation transport (OCT) inhibitor, quinine (Sigma, MO) for 2 h followed by co-incubation with rhodamine-6G. Quantitation of rhodamine-6G uptake was made at 488 nm excitation and 546 nm emission.

2.5. Immunofluorescence

The gKT structures were digested with collagenase A (2 mg/mL) (10103586001; Hoffmann-La Roche, NJ) for 10 min at 37 °C, washed with PBS immediately, then fixed 15 min with 4% paraformaldehyde, PBS-rinsed, and permeabilized 15 min with 0.5% Triton x-100. The fixed gKT structures were blocked with 5% BSA and sequentially incubated with primary and secondary antibodies. The following primary and secondary antibodies were used: rabbit ZO-1 (617330; Invitrogen, CA) (1:250), mouse E-cadherin (sc-8426; Santacruz Biotechnology, CA) (1:100), mouse anti-acetylated alpha-tubulin (T7451; Sigma MO) (1:50), rabbit Sodium Potassium ATPase pump (ab76020; Abcam, MA) (1:100), rabbit collagen IV (ab19808 Abcam, MA) (1:100), goat kidney injury molecule-1 (KIM-1) (AF1750; R&D systems, MN) (1:100), anti-rabbit (Alexa 488 or 546 conjugated, Invitrogen, CA), anti-mouse (Alexa 488 or 546 conjugated; Invitrogen, CA), anti-goat (Alexa 488 conjugated, Invitrogen, CA). For F-actin labeling gKT structures were labeled with rhodamine-phalloidin (Invitrogen, CA) (1:250). Following antibody incubations, gKT structure nuclei were counterstained with Hoechst (dsDNA) (Invitrogen, CA), mounted using ProLong Diamond Antifade (Invitrogen, CA) and imaged by confocal microscopy

(Zeiss LSM 510). All images were collected using ZEN lite 2.3 (black edition) and processed using ZEN lite 2.3 (blue version).

2.6. Apoptosis and necrosis detection assays

Induction of apoptosis and necrosis were evaluated using a tri-color live/apoptosis/necrosis kit (176749, Abcam, MA). Briefly, the live gKT structures were co-incubated at 37 °C for 30 min with CytoCalcein Violet (live), Phosphatidylserine sensor (Apoptotic) and 7-amino actinomycin D (7-AAD) (Necrotic) and imaged immediately in the assay buffer. Dye staining was quantitated by fluorescence of RIPA lysates of stained gKT structures. Excitation and emission wavelengths (Ex/Em) were set at 490/525 nm for Phosphatidylserine sensor; 546/647 nm for 7-AAD; 405/450 nm for CytoCalcein Violet. Values were normalized to total protein (BCA assay, Bio-Rad).

2.7. Immunoblotting

The array system was digested with collagenase A (2 mg/mL) at 37 °C for 20 min, and the released gKT structures were collected by centrifugation at 5000*g* at 4 °C for 10 min. The gKT structures were lysed in RIPA buffer, and cell lysates clarified by centrifugation at ~13000*g* for 15 min at 4 °C. Equal amounts of proteins were separated on a 4–20% reducing gel, transferred to a Polyvinylidene difluoride (PVDF) membrane (Bio-Rad, USA), and probed with KIM-1 antibody (1:500) (R&D systems, MN) (1:500). The membrane was then incubated with horseradish peroxidase (HRP) conjugated anti-goat secondary antibody (1: 4000) (sc2020; Santa Cruz Biotechnology, CA) and developed using a chemiluminescent-based substrate (Super Signal West Dura, ThermoFisher, MA). Total beta-actin (1:4000) (sc47778; Santa Cruz Biotechnology, CA) level was used as loading controls.

2.8. Morphometric and statistical analyses

Three array platforms together containing more than 100 gKTs were used for structural analysis. Bifurcating structures were defined as branching tubules. Structures of width within the range of pre-defined micropattern features and without any branching were defined as tubules. Spherical cell clusters were defined as spheroid structures. Branching structures, tubules and spheroids were counted from 10×-magnified images. The largest width along the length of the gKT structure was defined as tubular diameter and compared with similar dimensions measured after forskolin treatment for analysis of tubule dilation/ cyst transformation.

All statistical analyses were performed using one-way analysis of variance. When statistical significance was seen, the Student-Newman-Keuls test was used to find group differences. Statistical significance was set at a minimal value of $p < 0.05$. All calculations were made using Graph Pad Prism Version 6, and all values were reported as a mean ± standard deviation.

3. Results

3.1. Tissue geometry guided tubule array in an extracellular matrix-based microenvironment

To build a system amenable both to disease studies and to high-throughput screening, we incorporated *in vivo*-like physicochemical cues to emulate pathological changes in a homogeneous array platform scalable for high-throughput. A schematic representation of the stepwise procedure for developing the tubule array is shown in Fig. 1.

With mIMCD3 cells as our screening cell line, we determined the compatibility of our approach to guiding cells by replica-molded ECM with the morphological and structural qualities of kidney tubules. By monitoring tissue-dynamics on different ECM compositions, we noted specific ECM-dependent tissue outcomes. With collagen I matrix (3 mg/mL), cells extend out beyond the micropattern edges, forming un-organized tubular networks in the ECM between the micropatterns and generating overlapping structures by day 5 (Fig. 2A, D, and H). In contrast, in matrigel matrix the cells re-organized and collapsed all the micropatterns, leading to spheroid-like structural maturation (Fig. 2B, E, and H). In mixed collagen plus matrigel, cells remained within the guided-tissue geometry of the 3D micropatterns and matured as homogenous tubule structures (> 95% of the structures) with a central lumen and apical F-actin enrichment by Day 5 (Fig. 2C, F, and H). Human HK-2 proximal tubule cells in mixed collagen-matrigel matrix exhibited similar tubular structures within the guided-tissue geometry (Fig. 2I). However, HEK cells remained unorganized, as evaluated by F-actin and the tight junction localization, suggesting that the structural maturation in the gKT format is also dependent on cell-type properties (Fig. 2J).

3.2. Structural and functional features of gKT structures in the array

We evaluated whether our mIMCD3-based gKT structures in the array exhibit asymmetric polarized organization using marker-proteins such as E-cadherin (basolateral), ZO-1 (apical), Na^+K^+-ATPase pump (basolateral), acetylated alpha-tubulin (cilia – apical), and F-actin (apical enrichment). The Z-plane scanning of mIMCD3 gKT structures stained for E-cadherin and ZO-1 showed that the E-cadherin exhibited a basolateral distribution in all image-planes of the structure, while the ZO-1 was absent at the outer plane (top plane) and appeared from the inner plane (middle plane) onwards with an apical distribution towards the lumen (Fig. 3A–C and supplemental video 1). The cross-section plane image further confirmed the closed nature of structures and the presence of a central lumen in it (Fig. 3D). The other tested markers — Na^+K^+-ATPase, Collagen IV (basal), acetylated alpha-tubulin (Cilia), and F-actin —also exhibited their characteristic patterns (Fig. 3E and F). Similarly, gKT structures developed using HK-2 cells also displayed the expected distribution of tested marker proteins: Na^+K^+-ATPase pump, acetylated alpha-tubulin (Cilia), and F-actin (Fig. 3G), indicating that the gKTs derived from both cell types recapitulate typical kidney tubule-like asymmetric polarization.

Supplementary video related to this article can be found at https://doi.org/10.1016/j.biomaterials.2018.07.059.

Next, we tested the ability of HK-2 cell gKTs to perform functional features of kidney tubules by probing for their ability to transport organic anions [14–16]. To this end, the gKT array structures were exposed to Propidium Iodide (PI) to differentiate between dead and live cells, and to 6-Carboxy Fluorescein (6-CF) to evaluate 6-CF transport and its selectivity. Our results showed mutually exclusive staining for 6-CF and PI in the gKT structures (Fig. 4A and B). Moreover, we noted that 6-CF transport is sensitive to probenecid, an organic anion transport (OAT) protein family inhibitor [14–16]. Although some distortion of gKT structures was seen due to probenecid incubation for 2 h, the lack of propidium iodide staining or uptake in these cells indicates their continued viability, and the reduction in 6-CF uptake by probenecid co-incubation suggests inhibitory specificity for anion transport. Similarly, we tested for organic cation transport in gKT structures by uptake of rhodamine-6G [17]. Our results showed that the gKT structures exhibited rhodamine-6G uptake that are responsive to quinine, an organic cation transport (OCT) protein family inhibitor (Fig. 4C–D). Thus, our gKT structures express functional properties of kidney tubules as evaluated by small solute transport.

3.3. Cystic kidney disease modeling in the array

Kidney tubules display precisely controlled geometry subject to dysregulation in various pathological conditions [6,18,40–42]. Cystic kidney diseases are a clinically important group of diseases exemplifying the importance of control over tissue geometry for normal kidney functions [18,19,40–42]. Multiple studies have indicated that increases in intracellular cyclic adenosine-mono-phosphate (cAMP) levels drive progressive transformation from tubules to cysts [18]. In the present study, we treated our mIMCD3-based gKT structures with cAMP elevators such as forskolin and monitored alterations in the tubule structure. Bright field images of the tubules (Fig. 5A–C) show that forskolin treatments transform the tubules in the array into progressively dilating or cystic structures, as opposed to untreated control tubules. Quantitation of these structural changes showed that the forskolin treatment promoted tubule dilation in almost all the tubular structures with a higher degree of homogeneity than in regular 3D gel culture (Fig. 5D and E). This forskolin-induced change in tubule dilation is blocked by co-treatment with cation-Cl^- cotransporter inhibitor Bumetanide (Fig. 5C and E). Thus, our gKT array offers a homogenous tubule structure platform, capable of recapitulating in real time the disease-associated structural changes of cystic kidney disease. We tested whether this transformation is accompanied by changes in cell polarity using marker proteins such as ZO-1, E-cadherin, and Na^+K^+ATPase. The transformed structures exhibited normal apical ZO-1 and basolateral Na^+K^+-ATPase staining, whereas E-cadherin is weakly expressed and distributed throughout the cytoplasm in some regions of the cystic structures (Fig. 5F and G).

3.4. Acute kidney injury (AKI) disease modeling in the array

AKI is a clinical syndrome characterized by a rapid loss of renal function together with the accumulation of waste products such as urea. While the etiology of AKI in most cases can be multi-factorial, recent epidemiological studies have highlighted that kidney injury due to nephrotoxic drugs contributes to roughly 25% of all cases [20]. Cisplatin is a commonly used chemotherapeutic drug that often leads to nephrotoxicity [21]. To model drug-induced AKI in our system, we treated HK-2 cell gKT structures with cisplatin for 24 h and

evaluated changes associated with tubule injury. Analysis of the apoptotic (phosphatidylserine sensor) and necrotic (7-amino actinomycin D) markers showed that cisplatin treatments induced cell death in a dose-dependent manner (Fig. 6A and B). Induced cell death was accompanied by induction of previously reported kidney injury markers such as KIM-1 with *in vivo* tissue-like localization (predominantly apical), suggesting gKT structures can emulate features of kidney injury (Fig. 6C and D). We next searched for evidence of morphological abnormalities associated with the cisplatin-induced kidney injury. We observed a complete loss of F-actin apical polarization accompanied by the presence of hollow gaps in the kidney tubule structures and cell debris and clusters in the tubule lumen, consistent with key pathophysiological features of kidney tubule injury (Fig. 6D) [21–24].

4. Discussion

Multiple technologies have been used to develop *in vitro* kidney tubule systems, particularly those modeling the proximal tubule. 3D bioprinting offers a tubular channel with fluid flow, albeit of much larger diameter than the kidney tubule [25]. Microfluidic systems constitute a platform offering accurate quantitation of transport functions but have lacked the tubular shape [10,11]. Tissue-engineered scaffold-based approaches can provide long-term durability [5]. Kidney organoids offer a comprehensive platform for studying different nephron segments, but sometimes with impure preparations contaminated with cell types such as neurons [26,27]. The organ-on-chip technology recapitulates fluid flow in a tubule of diameter similar to that of kidney tubules but extrapolates outcomes from a single tubule segment [28]. Undoubtedly, these 3D *in vitro* tissue systems have incrementally advanced the field towards the development of models relevant to disease research and/or drug testing. However, to truly bridge the gap between animal models and 2D culture in disease pathophysiology studies, and for drug testing in pre-clinical applications, we envisioned that an *in vitro* tubule system should offer fluid flow through multiple homogenous nephron segments of physiological dimensions.

As a critical step towards this goal, in the present study, we have utilized lithography procedures and micropatterned ECM with kidney tubule dimensions in a 3D array configuration. Quantitative profiling on kidney ECM composition has indicated that collagen I, collagen IV and laminin are the major components of kidney ECM [13]. We studied mIMCD3 cells and HK-2 cells widely used in renal cell biology and ECM components comparable with kidney ECM. We found that when collagen I alone was used to form the pattern, the cells branch from the edges and form unorganized tubular networks. In contrast, when matrigel was used, the patterns are collapsed within 24 h, and cells formed spheroid–like structures without any branching. The patterns were no longer visibly present by 24 h. We believe that matrigel alone does not have the sufficient mechanical load-bearing capacity for the tissue maturation, and thus the ECM was remodeled and the entire patterned structures collapsed.

Therefore we used a combination of collagen-matrigel, which facilitated homogenous tubule formation with minimal variation from the pre-programmed kidney tubule dimension. We believe that the matrigel in the combination inhibited the branching from the edges and the presence of collagen I conferred necessary mechanical properties and facilitated the tubule

formation within the micropatterned geometry. Furthermore, the lack of proper tubule organization by HEK cells in the combined collagen-matrigel matrix confirms that matrix composition and tissue geometry in 3D alone does not determine tubulogenesis outcomes, which reflect inherent cell morphogenetic capacity to form polarized structures are also equally important. Thus the system guides the cells' morphogenesis with the *in vivo*-like physical cues and chemical cues and forms the tubule structures — guided kidney tubule (gKT) structures.

We have tested the differentiation state of gKT structures produced in our system using the localization of specific marker proteins. The results showed that the gKT structures, both from HK-2 cells and mIMCD3 cells, exhibited kidney tissue-like localization of all tested marker proteins, suggesting a mature state of the gKT structures, with kidney tubule-like asymmetric organization. However, in a few instances, we do also note some positive nuclear stain in the luminal region that is negative for marker proteins. We believe this might be cell debris remnants that are usually noted during lumen formation and in the process of getting cleared. Alternatively, these cells could have dislodged during the collagenase digestion step of processing for imaging. In any case, our results indicate the closed nature of our structures with a central luminal region and asymmetric organization.

We have also shown that our gKT structures are functionally competent, as evidenced by transport of the organic anion, 6-CF and organic cation, rhodamine-6G. Although different nephron segments have different transport properties, proximal tubules are highest in organic anion and cation transport activity. We, therefore, evaluated 6-CF and rhodamine-6G transport in gKT structures of proximal tubule-like HK-2 cells. Selective 6-CF uptake sensitive to inhibition by the organic anion transporter inhibitor, probenecid, and rhodamine-6G uptake sensitive to organic cation inhibitor, quinine, suggest the specificity of our measured 6-CF and rhodamine-6G transport. Earlier expression studies have indicated that 2D-cultured HK-2 cells lack expression of OAT, OAT3 and OCT transporter proteins [29]. The incomplete inhibition of 6-CF uptake by probenecid and rhodamine-6G uptake by quinine in our system suggests possible functional compensation between family member proteins [16] or tubular morphology in our system could have modulated their expression profiles as seen in organ cultures [30]. Alternatively, It is also possible that the inhibitor concentration is insufficient for complete inhibition of the multiple OAT and OCTs and other transporters for which 6-CF and rhodamine-6G is the substrate. Future experiments directed towards protein expression analysis and validation of OAT and OCT protein activity in the gKT structures will allow a better understanding of kidney tubule transport function particularly in the context of drug transport.

We have also demonstrated the suitability of the gKT system for disease studies by simulating cystic kidney disease and drug-induced AKI, thus providing a platform to evaluate the underlying molecular mechanisms or test drugs in a disease kidney-like tissue. Multiple reports have shown that progressive tubule-to-cyst expansion and collapse of neighboring kidney parenchyma are hallmarks of several cystic kidney diseases currently targeted for drug discovery [31–33]. Local microenvironment changes can also drive cyst progression and modulate or disrupt normal apicobasal cell polarity [34–36]. In accordance with these reports, forskolin treatment in our gKT array produced progressive tubule-to-cyst

expansion. Furthermore, the kidney-like ECM microenvironment composed of collagen I and matrigel in our system facilitated continuous cyst progression, with the altered polarity of expression of E-cadherin [5,34]. The lack of apical membrane localization of Na^+K^+-ATPase pump, a reversed polarity sometimes seen in polycystic kidney diseases [37], might reflect use of “normal” tissue culture cells in our system as opposed to mutant cells present in cysts of patients, or could reflect altered downstream events in *in vitro* vs *in vivo* cyst progression.

Previous studies in mouse models have used cisplatin doses ranging from 10 to 30 mg/kg [38]. It was shown that the pathophysiology of cisplatin-induced AKI involves kidney tubule injury with the induction of apoptosis and necrosis [21]. Although the dose range used in this study may not fully mimic the doses used in mouse studies or clinical practice [38], our results show that the dose inducing significant changes in gKT structures is similar to that injuring proximal tubules *in vivo*, including induction of apoptosis and necrosis [23]. Furthermore, the presence of actin localization defects and KIM-1 upregulation and apical localization in the cisplatin-treated gKT structures further confirms gKT relevance as a reductionist model of human kidney suitable for contributing to understanding various mechanisms of drug-induced renal tubular injury [23]. Thus, overall, the studies presented here establish the relevance of gKT structures to kidney tubules and serve as the proof-of-concept for their use in disease research and pre-clinical drug testing.

Recent advances in iPSC technologies have improved disease modeling including kidney diseases with the advantage of personalized to individual patients [26]. IPSc-derived kidney-organoid models develop connected tubules and have been used to study phenotypic transformations in disease conditions [26]. However, at the current stage, the kidney-organoid models have significant batch-to-batch variability and develop contaminating cells such as neurons in the system, indicating that the differentiation procedures to develop kidney-organoids need more refinement [26,27,39]. In contrast, our guided system, though made of differentiated cells, yields homogenous structures, and can be extended to include the connections between individual structures by altering the micropattern configuration. Moreover, with the new advances in the iPS technologies, one could imagine that combining iPS cells with our guided approach would lead to new avenues in kidney tissue modeling in the future.

Thus, these gKT structures represent a significant advance towards models with organotypic homogenous kidney tubules for the study of disease and drug testing. Future studies will introduce lumenal fluid flow to gKT structures and will construct axial connections between gKT structures built from proximal and distal nephron segments, to better mimic the kidney tubular network. One can further envision future co-culture of multiple cell types within the gKT geometry, including peritubular endothelial cells to create “vascularized” gKT structures.

5. Conclusion

We report a novel gKT array system that includes physicochemical cues in 3D culture to guide kidney tubule cells to form uniform tubular structures. The gKT array system offers

multiple technological improvements over existing 3D culture methods, including (1) control over tubule geometry at the pre-programmable design stage, yielding kidney tubule dimensions (~50 μm outer diameter) of physiological scale; (2) synchronized growth of all structures in the system; (3) simultaneous or sequential disease modeling and drug testing with the same platform, and (4) mid-throughput format expandable to a high-throughput configuration.

Supplementary Material

Refer to Web version on PubMed Central for supplementary material.

Acknowledgments

We would like to thank the members of the Zhou Lab and the Harvard Center for Polycystic Kidney Disease Research (P50DK074030) for scientific discussions and support. We would like to thank Calixto Saenz from the microfluidics facility at the Department of Systems Biology at Harvard Medical School, for micropattern preparation guidance and suggestions. The authors also thank Celeste Nelson from Princeton University for sharing some of their micropatterns in our trial experiments. This work was supported by grants from the National Institutes of Health, United States (RO1DK099532, RO1DK51050, and RO1DK40703), Department of Defense (W81XWH-16-1-0617), American Heart Association (16GRT31380023), and a grant from the Harvard Stem Cell Institute, United States to J. Z. B.S. was, in part, supported by a T32 Nephrology Training Grant from National Institute of Health, United States (DK007199).

References

[1]. Hofmeister AF, Kömhoff M, Weber S, Grgic I, Disease modeling in genetic kidney diseases: mice, Cell Tissue Res 369 (2017) 159–170, 10.1007/s00441-017-2639-3. [PubMed: 28601904]

[2]. Yang H-C, Zuo Y, Fogo AB, Models of chronic kidney disease, Drug Discov. Today Dis. Model 7 (2010) 13–19, 10.1016/j.ddmod.2010.08.002.Models.

[3]. Rimann M, Graf-Hausner U, Synthetic 3D multicellular systems for drug development, Curr. Opin. Biotechnol 23 (2012) 803–809, 10.1016/j.copbio.2012.01.011. [PubMed: 22326911]

[4]. Breslin S, O'Driscoll L, Three-dimensional cell culture: the missing link in drug discovery, Drug Discov. Today 18 (2013) 240–249, 10.1016/j.drudis.2012.10.003. [PubMed: 23073387]

[5]. Subramanian B, Rudym D, Cannizzaro C, Perrone R, Zhou J, Kaplan DL, Tissue-engineered three-dimensional in vitro models for normal and diseased kidney, Tissue Eng. Part A 16 (2010) 2821–2831, 10.1089/ten.tea.2009.0595. [PubMed: 20486787]

[6]. Little M, Georgas K, Pennisi D, Wilkinson L, Kidney development: two tales of tubulogenesis, Curr. Top. Dev. Biol 90 (2010) 193–229, 10.1016/S0070-2153(10)90005-7. [PubMed: 20691850]

[7]. Lawrence ML, Chang C-H, Davies JA, Transport of organic anions and cations in murine embryonic kidney development and in serially-reaggregated engineered kidneys, Sci. Rep 5 (2015) 9092, 10.1038/srep09092. [PubMed: 25766625]

[8]. Nieskens TTG, Wilmer MJ, Kidney-on-a-chip technology for renal proximal tubule tissue reconstruction, Eur. J. Pharmacol 790 (2016) 46–56, 10.1016/j.ejphar.2016.07.018. [PubMed: 27401035]

[9]. Giles RH, Ajzenberg H, Jackson PK, 3D spheroid model of mIMCD3 cells for studying ciliopathies and renal epithelial disorders, Nat. Protoc 9 (2014) 2725–2731, 10.1038/nprot.2014.181. [PubMed: 25356583]

[10]. Jang K-J, Mehr AP, Hamilton GA, McPartlin LA, Chung S, Suh K-Y,Ingber DE, Human kidney proximal tubule-on-a-chip for drug transport and nephrotoxicity assessment, Integr. Biol 5 (2013) 1119, 10.1039/c3ib40049b.

[11]. Vedula EM, Alonso JL, Arnaout MA, Charest JL, A microfluidic renal proximal tubule with active reabsorptive function, PLoS One 12 (2017) 1–15, 10.1371/journal.pone.0184330.

[12]. Nelson CM, Vanduijn MM, Inman JL, Fletcher DA, Bissell J, NIH Public Access 314 (2010) 298–300, 10.1126/science.1131000.Tissue.

[13]. Nagao RJ, Xu J, Luo P, Xue J, Wang Y, Kotha S, Zeng W, Fu X, Himmelfarb J,Zheng Y, Decellularized human kidney cortex hydrogels enhance kidney micro-vascular endothelial cell maturation and quiescence, Tissue Eng. Part A 22 (2016) 1140–1150, 10.1089/ten.tea.2016.0213. [PubMed: 27481445]

[14]. Otani N, Ouchi M, Hayashi K, Jutabha P, Anzai N, Roles of organic anion transporters (OATs) in renal proximal tubules and their localization, Anat. Sci. Int 92 (2017) 200–206, 10.1007/s12565-016-0369-3. [PubMed: 27614971]

[15]. Huo X, Liu K, Renal organic anion transporters in drug–drug interactions and diseases, Eur. J. Pharmaceut. Sci 112 (2018) 8–19, 10.1016/j.ejps.2017.11.001.

[16]. Burckhardt G, Drug transport by organic anion transporters (OATs), Pharmacol. Ther 136 (2012) 106–130, 10.1016/j.pharmthera.2012.07.010. [PubMed: 22841915]

[17]. Ugwu MC, Pelis R, Esimone CO, Agu RU, Fluorescent organic cations for human OCT2 transporters screening: uptake in CHO cells stably expressing hOCT2, ADMET DMPK 5 (2017) 135, 10.5599/admet.5.2.389.

[18]. Harris PC, Torres VE, Review series Genetic mechanisms and signaling pathways in autosomal dominant polycystic kidney disease, J. Clin. Invest 124 (2014) 2315–2324, 10.1172/JCI72272.Most. [PubMed: 24892705]

[19]. Lanktree MB, Chapman AB, New treatment paradigms for ADPKD: moving towards precision medicine, Nat. Rev. Nephrol 13 (2017) 750–768, 10.1038/nrneph.2017.127. [PubMed: 28989174]

[20]. Kaushal GP, Shah SV, Challenges and advances in the treatment of AKI, J. Am. Soc. Nephrol 25 (2014) 877–883, 10.1681/ASN.2013070780. [PubMed: 24480828]

[21]. Ozkok A, Edelstein CL, Pathophysiology of cisplatin-induced acute kidney injury, BioMed Res. Int 2014 (2014), 10.1155/2014/967826.

[22]. Xu Y, Ma H, Shao J, Wu J, Zhou L, Zhang Z, Wang Y, Huang Z, Ren J, Liu S,Chen X, Han J, A role for tubular necroptosis in cisplatin-induced AKI, J. Am. Soc. Nephrol 26 (2015) 2647–2658, 10.1681/ASN.2014080741. [PubMed: 25788533]

[23]. van Timmeren MM, Bakker SJL, Vaidya VS, Bailly V, a Schuurs T, Damman J, a Stegeman C, Bonventre JV, van Goor H, Tubular kidney injury molecule-1 in protein-overload nephropathy, Am. J. Physiol. Ren. Physiol 291 (2006) F456–F464, 10.1152/ajprenal.00403.2005.

[24]. Ichimura T, Kidney injury molecule-1: a tissue and urinary biomarker for nephrotoxicant-induced renal injury, AJP Ren. Physiol 286 (2004) 552F–563F, 10.1152/ajprenal.00285.2002.

[25]. Homan KA, Kolesky DB, Skylar-Scott MA, Herrmann J, Obuobi H, Moisan A, Lewis JA, Bioprinting of 3D convoluted renal proximal tubules on perfusable chips, Sci. Rep 6 (2016) 1–13, 10.1038/srep34845. [PubMed: 28442746]

[26]. Freedman BS, Brooks CR, Lam AQ, Fu H, Morizane R, Agrawal V, Saad AF, Li MK, Hughes MR, Vander Werff R, Peters DT, Lu J, Baccei A, Siedlecki AM, Valerius MT, Musunuru K, McNagny KM, Steinman TI, Zhou J, Lerou PH, Bonventre JV, Modelling kidney disease with CRISPR-mutant kidney organoids derived from human pluripotent epiblast spheroids, Nat. Commun 6 (2015) 1–13, 10.1038/ncomms9715.

[27]. Takasato M, Er PX, Chiu HS, Maier B, Baillie GJ, Ferguson C, Parton RG, Wolvetang EJ, Roost MS, De Sousa Lopes SMC, Little MH, Kidney organoids from human iPS cells contain multiple lineages and model human nephrogenesis, Nature 526 (2015) 564–568, 10.1038/nature15695. [PubMed: 26444236]

[28]. Weber EJ, Chapron A, Chapron BD, Voellinger JL, Lidberg KA, Yeung CK, Wang Z, Yamaura Y, Hailey DW, Neumann T, Shen DD, Thummel KE, Muczynski KA, Himmelfarb J, Kelly EJ, Development of a microphysiological model of human kidney proximal tubule function, Kidney Int 90 (2016) 627–637, 10.1016/j.kint.2016.06.011. [PubMed: 27521113]

[29]. Jenkinson SE, Chung GW, van Loon E, Bakar NS, Dalzell AM, Brown CDA, The limitations of renal epithelial cell line HK-2 as a model of drug transporter expression and function in the proximal tubule, Pflugers Arch. Eur. J. Physiol (2012) 1–11, 10.1007/s00424-012-1163-2.

[30]. Sweet DH, Eraly SA, Vaughn DA, Bush KT, Nigam SK, Organic anion and cation transporter expression and function during embryonic kidney development and in organ culture models, Kidney Int 69 (2006) 837–845, 10.1038/sj.ki.5000170. [PubMed: 16518343]

[31]. Hanaoka K, Guggino WB, cAMP regulates cell proliferation and cyst formation in autosomal polycystic kidney disease cells, J. Am. Soc. Nephrol 11 (2000) 1179–1187 1046–6673/1107–1179. [PubMed: 10864573]

[32]. Montesano R, Ghzili H, Carrozzino F, Rossier BC, Féraille E, cAMP-dependent chloride secretion mediates tubule enlargement and cyst formation by cultured mammalian collecting duct cells, Am. J. Physiol. Ren. Physiol 296 (2009) F446–F457, 10.1152/ajprenal.90415.2008.

[33]. Torres VE, Harris PC, Strategies targeting cAMP signaling in the treatment of polycystic kidney disease, J. Am. Soc. Nephrol 25 (2014) 18–32, 10.1681/ASN.2013040398. [PubMed: 24335972]

[34]. Subramanian B, Ko WC, Yadav V, DesRochers TM, Perrone RD, Zhou J, Kaplan DL, The regulation of cystogenesis in a tissue engineered kidney disease system by abnormal matrix interactions, Biomaterials 33 (2012) 8383–8394, 10.1016/j.biomaterials.2012.08.020. [PubMed: 22940218]

[35]. Cruz NM, Song X, Czerniecki SM, Gulieva RE, Churchill AJ, Kim YK, Winston K, Tran LM, Diaz MA, Fu H, Finn LS, Pei Y, Himmelfarb J, Freedman BS, Organoid cystogenesis reveals a critical role of microenvironment in human polycystic kidney disease, Nat. Mater 16 (2017), 10.1038/nmat4994.

[36]. Lee K, Boctor S, Barisoni LMC, Gusella GL, Inactivation of integrin- 1 prevents the development of polycystic kidney disease after the loss of Polycystin-1, J. Am. Soc. Nephrol 26 (2015) 888–895, 10.1681/ASN.2013111179. [PubMed: 25145933]

[37]. Wilson PD, Sherwood a C., Palla K, Du J, Watson R, Norman JT, Reversed polarity of Na(+) - K(+) -ATPase: mislocation to apical plasma membranes in polycystic kidney disease epithelia, Am. J. Physiol 260 (1991) F420–F430, 10.1152/ajprenal.1991.260.3.F420. [PubMed: 1848046]

[38]. Sharp CN, Siskind LJ, Developing better mouse models to study cisplatin-induced kidney injury, Am. J. Physiol. Ren. Physiol (2017), 10.1152/ajprenal.00285.2017ajprenal.00285.2017.

[39]. Morizane R, Lam AQ, Freedman BS, Kishi S, Valerius MT, Bonventre JV, Nephron organoids derived from human pluripotent stem cells model kidney development and injury, Nat. Biotechnol 33 (2015) 1193–1200, 10.1038/nbt.3392. [PubMed: 26458176]

[40]. Zhou J, Pei Y, Autosomal dominant polycystic kidney disease, in: Mount DB, Pollak MR(Eds.), The Molecular and Genetic Basis of Kidney Disease. A Companion to Brenner and Rector's The Kidney, Saunders/Elsevier, Philadelphia, 2007, pp. 85–171.

[41]. Zhou J, Polycystins and primary cilia, primers for cell cycle progression, Ann. Rev. Physiol 71 (2009) 83–113. [PubMed: 19572811]

[42]. Zhou J, Pollak M, Polycystic kidney disease and other inherited tubular disorders, in: Kasper D, Fauci A, Hauser S, Longo D, Jameson JL, Loscalzo J (Eds.), Harrison's Principles of Internal Medicine, 20th edition, McGraw-Hill, New York, 2018, pp. 2150–2157.

HIGHLIGHTS

- *In vitro* system supporting organotypic homogenous kidney tubule formation.
- Matrix combination, Micro pattern features, and Cells intrinsic properties act as determinants of final tissue outcomes.
- Exhibits characteristic kidney disease transformations *in vitro*.
- Scalable to high throughput configuration for drug testing applications.

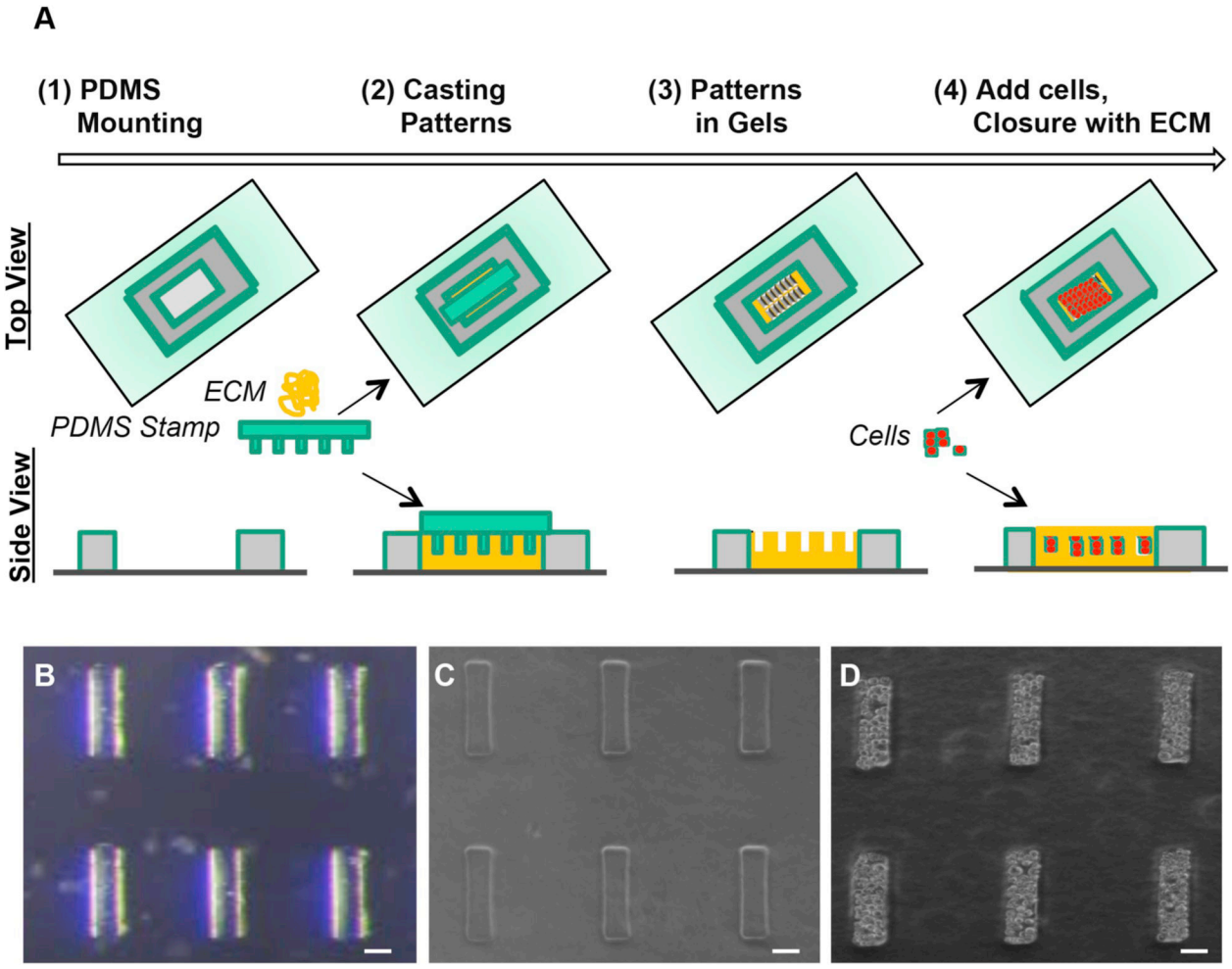

Fig. 1.

Guided Kidney Tubule (gKT) array set up. (A) Step-wise schematic representation of the gKT array set up. (B) Representative image of PDMS stamp with micropatterns used in the system. (C) After replica molding patterns in ECM (collagen-matrigel). (D) After cell delivery and ECM closure. Scale bars, 50 μm.

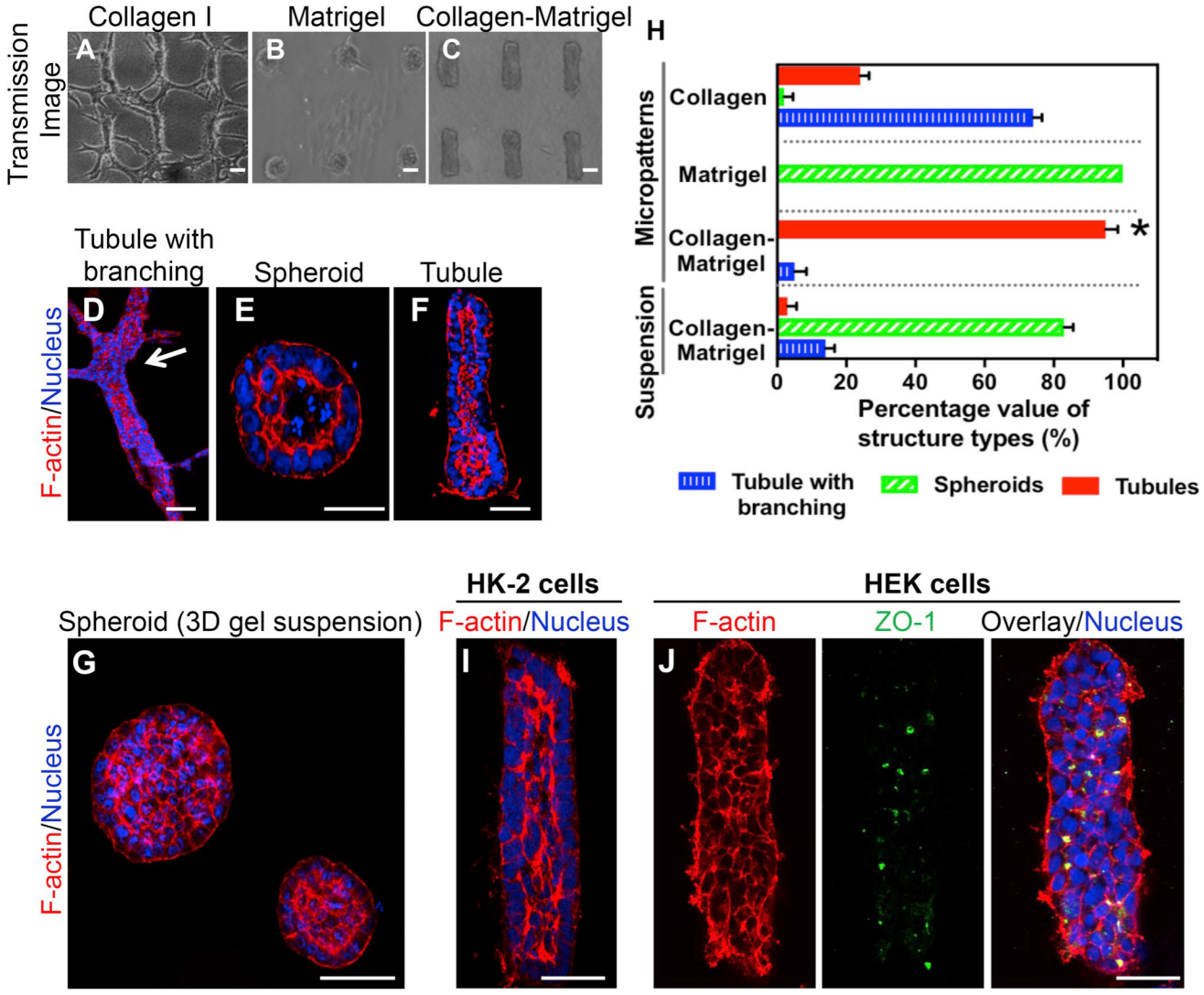

Fig. 2.

Effect of different ECM composition on tissue outcomes in the gKT array system. (A–G) Collagen I, Matrigel, or collagen-matrigel were used as ECM to form the gKT array system. mIMCD3 cells were seeded onto the preformed micropattern features in different ECM compositions and evaluated for changes in morphologic outcomes at day 5 after seeding. (A–C) Tissue patterns observed in the gKT system with different ECM composition. (A) Collagen-ECM induced tubules with branching structures. (B) Matrigel-ECM induced spheroid-like structures. (C) Collagen-matrigel-ECM-induced tubules in the range of micropattern dimensions (~50 μm diameter) and exhibited no terminal branching. (D–G) Representative individual structures grown with different ECM conditions, stained for F-actin (red) and nuclei (blue). (D) Tubule with branching structures. Branching area is highlighted (white arrow). (E) Spheroid structures. (F) Tubule in gKT array system. (G) Varying size spheroids in 3D collagen-matrigel suspension cultures. (H) Quantitation of different tissue patterns observed in the gKT system and 3D gel systems (n = 112 for collagen I; n = 124 for collagen-matrigel; n = 136 for matrigel; n = 103 for 3D gel

suspension). Homogenous tubules in the range of predefined micropattern dimensions were seen in the collagen-matrigel condition, whereas other ECM compositions and culture methods exhibited different tissue patterns and heterogeneous tissue outcomes (*$p < 0.01$ by one-way analysis of variance (ANOVA); tubules in micropatterned collagen-matrigel ECM vs tubules in other groups). (I & J) Cell type dependency in tubule formation in the gKT array system. HK-2 or HEK cells were used to form the gKT structures in collagen-matrigel ECM. HK-2 cells formed matured tubule structures (I), while no clear apical F-actin and ZO-1 were evident, indicating immaturity of the structures with HEK cells (J). Scale bars, 50 μm. (For interpretation of the references to color in this figure legend, the reader is referred to the Web version of this article.)

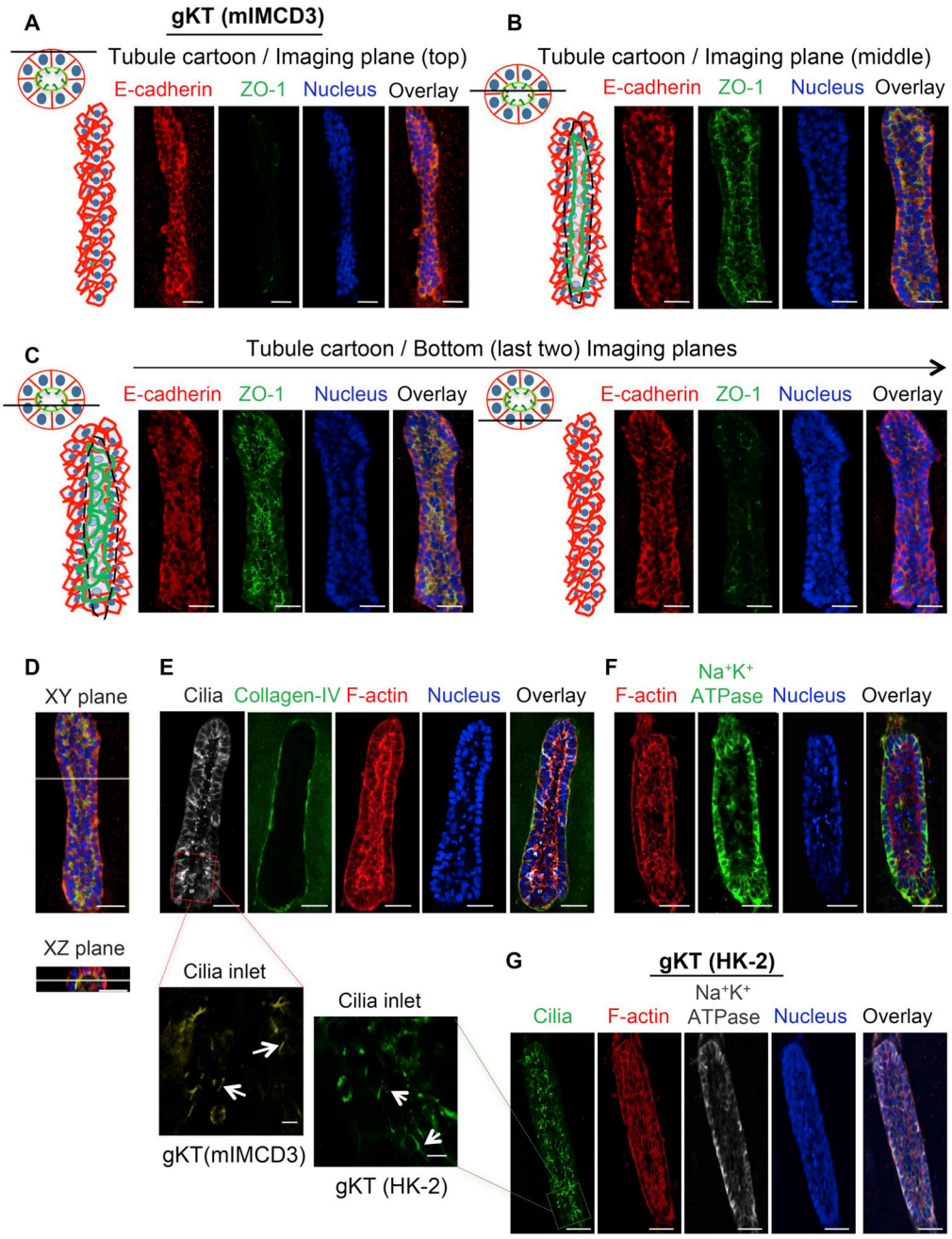

Fig. 3.

Evaluation of polarized organization in the gKT structures. gKT structural asymmetry was evaluated by specific marker protein localization. (A–E) Analysis of mIMCD3-based gKT structures. (A–C) Cartoon for the imaging plane of the gKT and the corresponding confocal Z-sections from a gKT structure stained for E-cadherin (basolateral) and ZO-1 (apical). (A) Cartoon for the imaging Z-section plane (coronal and cross-sectional planes) and top images of the gKT (coronal plane images). The line in the cartoon indicates the position of the imaging plane in the gKT (B) Cartoon for the imaging Z-section plane and middle plane images of the gKT (C) Cartoon for the imaging Z-section plane and bottom plane images of

the gKT. (D) Coronal (XY) and cross-section plane (XZ) images of the gKT. (E & F) Confocal images for marker proteins, cilia (acetylated alpha-tubulin) (apical), F-actin (enrichment in apical), collagen IV (basal), Na^+K^+-ATPase (basolateral) (G) Confocal images for marker proteins, F-actin, cilia and Na^+K^+-ATPase, from HK-2 cells-based gKT structure. Scale bars, 50 μm. High-magnification images of cilia inlets, corresponding to highlighted (red and green) box areas in cilia staining of E and G were provided as well. White arrows in them indicate cilia structures. mIMCD3-gKT cilia inlet image is pseudo-colored to yellow from the original gray image for enhancing contrast. Scale bars in them are 5 μm. (For interpretation of the references to color in this figure legend, the reader is referred to the Web version of this article.)

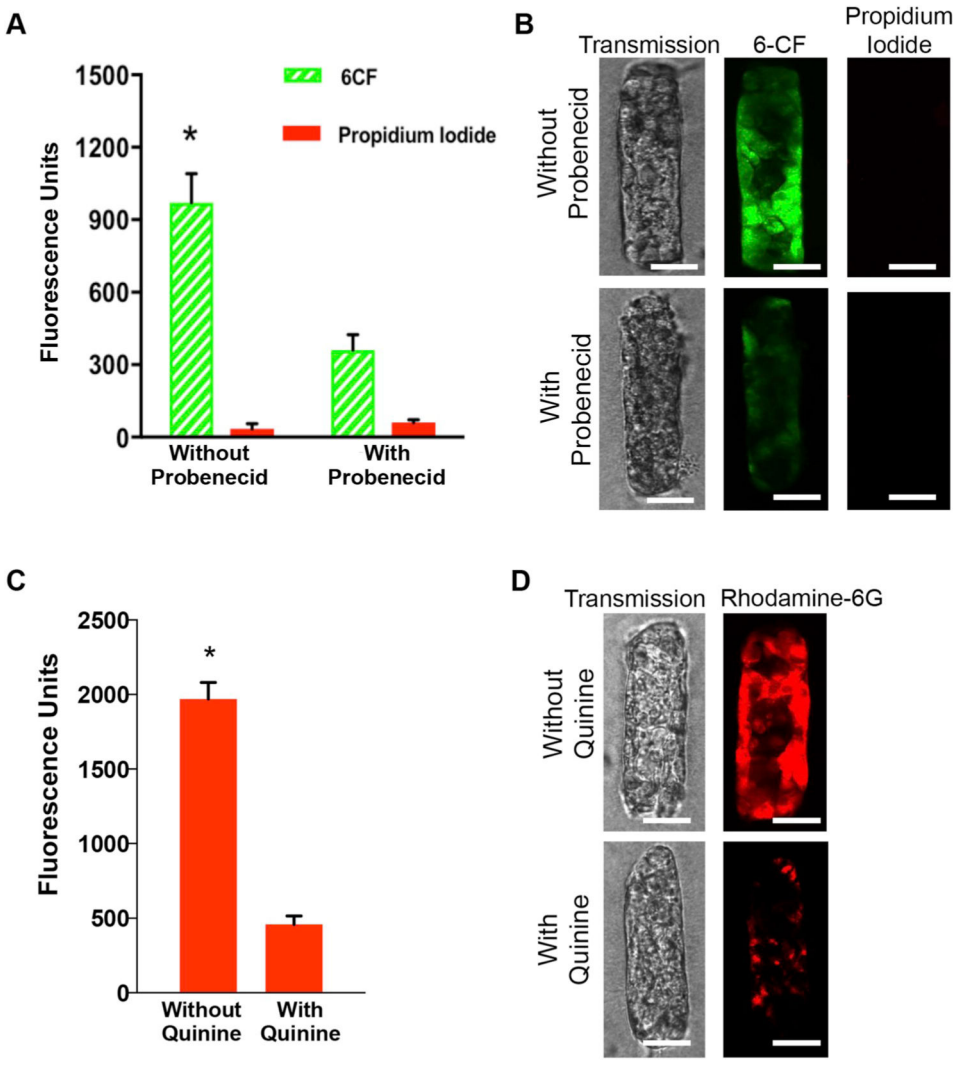

Fig. 4.

Evaluation of transport function in the gKT structures. Selective uptake of the organic anion, 6-Carboxy Fluorescein (6-CF) in HK-2 cell gKT structures. (A) Quantitation of uptake of 6-CF (2 μM) and propidium iodide (2 μM) without and with concurrent probenecid (2 mM) treatment. Values normalized to protein levels. 6-CF uptake was significantly reduced with probe-necid (*$p < 0.01$). No propidium iodide uptake was observed. (B) Representative confocal images of gKT for 6-CF and propidium iodide, in the absence (top panel) and presence of probenecid (bottom panel). (C) Quantitation of uptake of rhodamine-6G (50 μM) without and with concurrent quinine (500 μM) treatment. Values normalized to protein levels. Rhodamine-6G was significantly reduced with quinine (*$p < 0.01$).(D) Representative confocal images of gKT for rhodamine-6G in the absence (top panel) and presence of quinine (bottom panel). (B & D) Images were collected on unfixed cells. Scale bars, 50 μm.

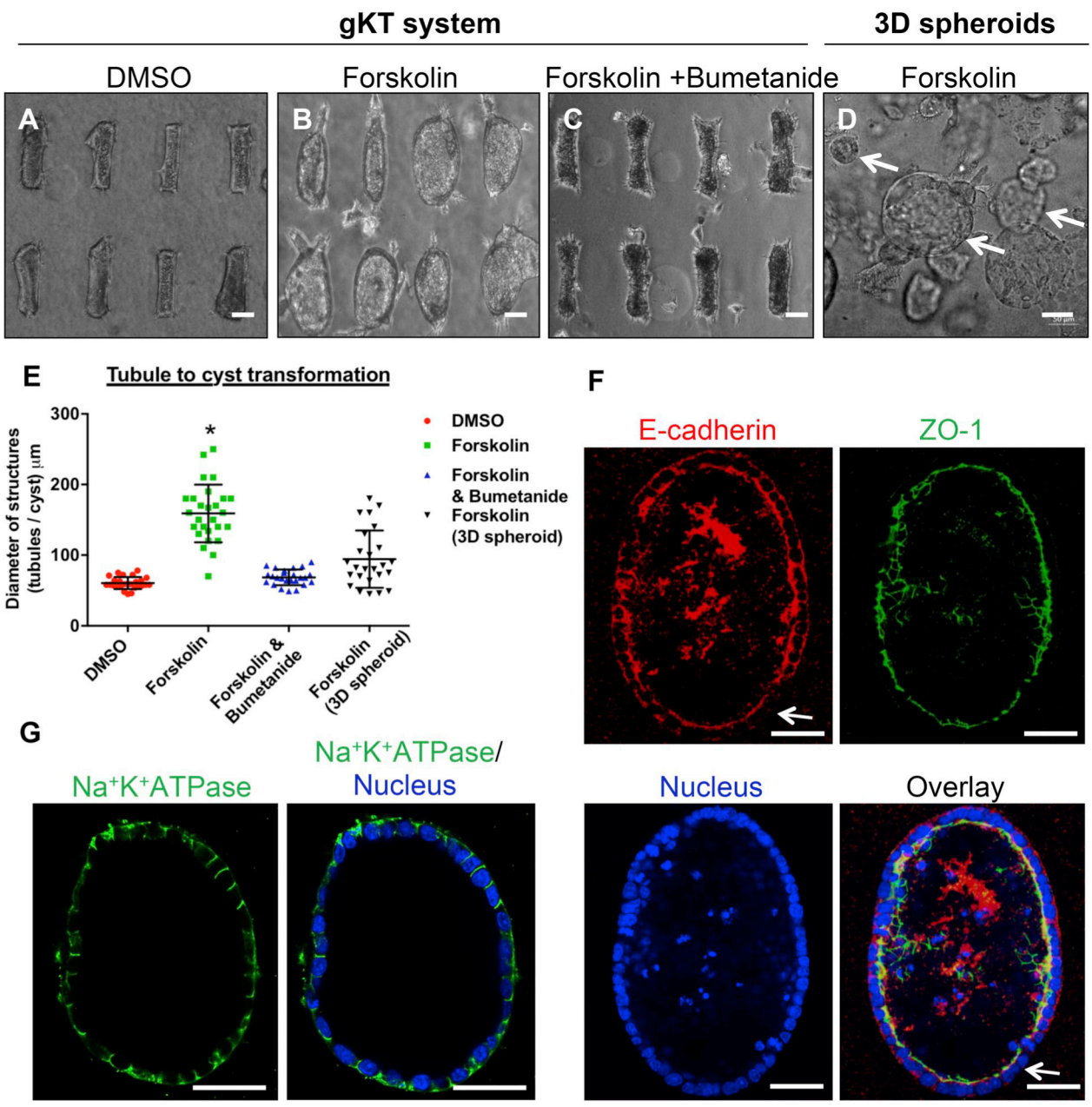

Fig. 5.

Cystic Kidney Disease modeling in the tubule array. (A–E) Tubule to cyst transformation was modeled in the array. All treatments were introduced at day 3 and images were collected at day 5. Structures are treated with (A) Dimethyl Sulfoxide (DMSO) (B) cAMP stimulator (forskolin) (C) Forskolin and NKCC1 inhibitor (bumetanide). Forskolin treatment caused tubules to undergo a cystic transformation, and co-treatment with bumetanide inhibited it. (D) Forskolin-treated spheroids in a 3D gel suspension culture for reference. Structures of varied sizes are highlighted (white arrows). Scale bar, 50 µm. (E) Quantitation of tubule or cyst diameter with indicated treatments. (*$p < 0.01$; forskolin-treated gKT vs. all other groups). (F & G) Marker protein (E-cadherin, ZO-1, and Na^+K^+-ATPase) evaluation in forskolin-treated conditions. No obvious change in ZO-1 and Na^+K^+-ATPase were noted.

Subtle changes (loss in some area) in E-cadherin distribution were noted (arrow highlights). Scale bars, 50 μm.

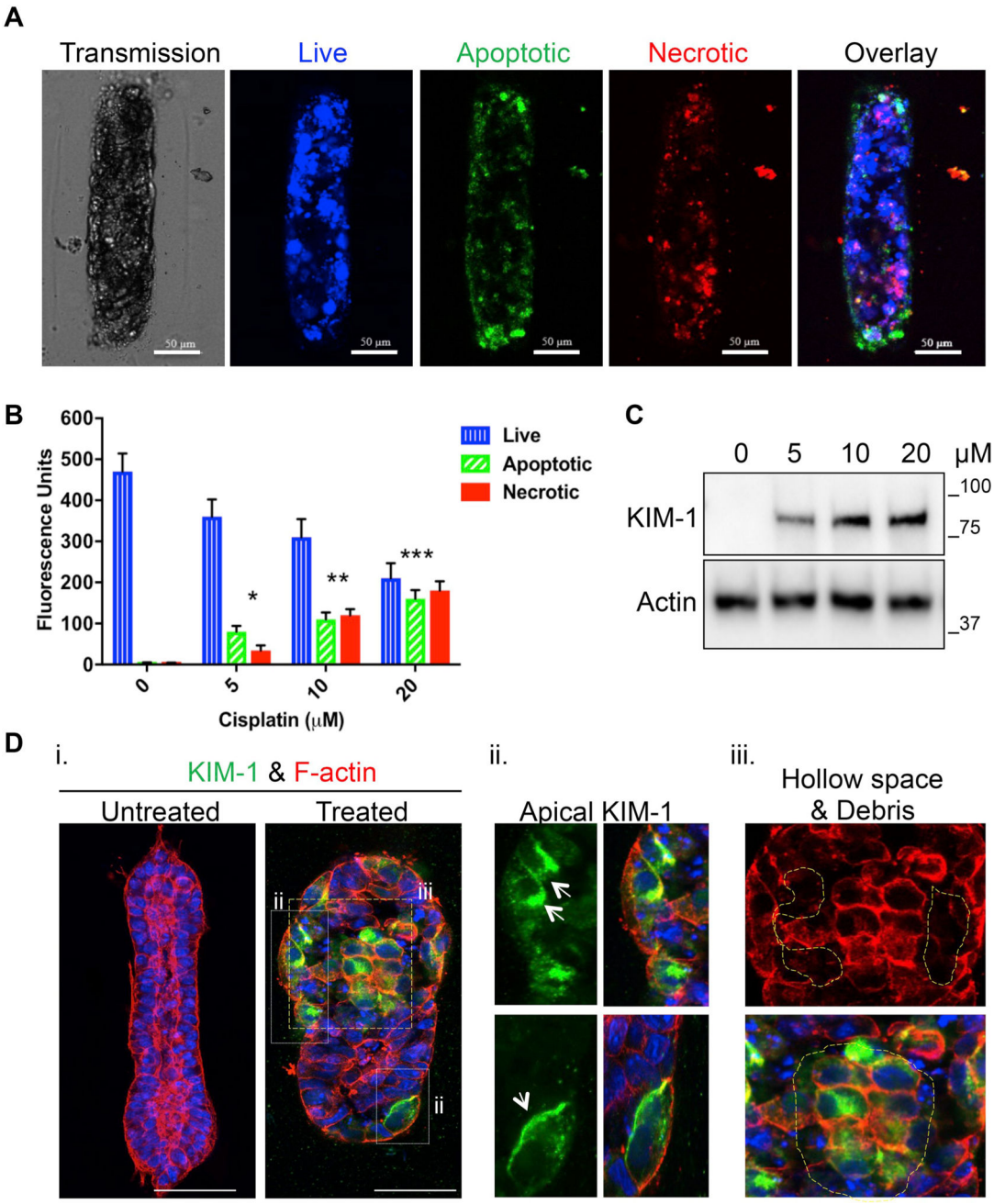

Fig. 6.

Acute Kidney Injury (AKI) modeling in gKT structures. Guided KT structures were treated with the indicated concentrations of cisplatin (5, 10 and 20 μM) for 24 hr on day 4 and evaluated for apoptosis and necrosis induction at the end of the 24 h treatment period. (A) Representative images are showing CytoCalcein Violet (cell permeable live cell marker), phosphatidylserine sensor (marker to evaluate loss of membrane asymmetry in apoptosis) and 7-AAD (DNA intercalating agent staining necrotic cells) staining in the structures after cisplatin treatment. The images presented were from gKT structures treated with 20 μM cisplatin. (B) Quantitation of apoptosis and necrosis in the gKT system. Values were

normalized to protein levels. A dose-dependent increase in apoptosis and necrosis was noted. (*$p < 0.01$, Apoptosis/Necrosis induction in 5 μM ($n = 121$) vs. untreated ($n = 116$); **$p < 0.05$ Apoptosis/Necrosis in 10 μM ($n = 104$) vs. 5 μM and untreated; ***$p < 0.05$, Apoptosis/Necrosis 20 μM ($n = 132$) vs. all other groups). (C & D) Cisplatin injury caused structural changes and induced expression of injury markers such as KIM-1 with proper localization. (C) Immunoblot analysis of gKT lysates showing a dose-dependent increase in KIM-1 expression. (D) (i) Confocal images of untreated and cisplatin-treated gKT structures stained for KIM-1 and F-actin. (ii) Area of white box from the treated panel (i) showing predominant apical localization of KIM-1 (arrow). (iii) Area of yellow box from the treated panel (i) showing structural deformation (loss of F-actin apical enriched distribution and hollow space formation due to cell death – yellow highlights) and luminal cell clusters and cell debris (white highlights). Scale bars, 50 μm. (For interpretation of the references to color in this figure legend, the reader is referred to the Web version of this article.)